Published in final edited form as:
J Immunol. 2010 March 15; 184(6): 3033–3042. doi:10.4049/jimmunol.0903712.

Endoplasmic Reticulum Aminopeptidase Associated with Antigen Processing Defines the Composition and Structure of MHC Class I Peptide Repertoire in Normal and Virus-Infected Cells

Nicolas Blanchard[*], **Takayuki Kanaseki**[*], **Hernando Escobar**[†], **Frédéric Delebecque**[*], **Niranjana A. Nagarajan**[*], **Eduardo Reyes-Vargas**[‡], **David K. Crockett**[†], **David H. Raulet**[*], **Julio C. Delgado**[†,‡], and **Nilabh Shastri**[*]

[*]Division of Immunology and Pathogenesis, Department of Molecular and Cell Biology, University of California, Berkeley, CA 94720

[†]ARUP Institute for Clinical and Experimental Pathology, University of Utah, Salt Lake City, UT 84112

[‡]Department of Pathology, University of Utah, Salt Lake City, UT 84112

Abstract

The MHC class I (MHC-I) molecules ferry a cargo of peptides to the cell surface as potential ligands for $CD8^+$ cytotoxic T cells. For nearly 20 years, the cargo has been described as a collection of short 8-9 mer peptides, whose length and sequences were believed to be primarily determined by the peptide-binding groove of MHC-I molecules. Yet the mechanisms for producing peptides of such optimal length and composition have remained unclear. In this study, using mass spectrometry, we determined the amino acid sequences of a large number of naturally processed peptides in mice lacking the endoplasmic reticulum aminopeptidase associated with Ag processing (ERAAP). We find that ERAAP-deficiency changed the oeuvre and caused a marked increase in the length of peptides normally presented by MHC-I. Furthermore, we observed similar changes in the length of viral peptides recognized by $CD8^+$ T cells in mouse CMV-infected ERAAP-deficient mice. In these mice, a distinct $CD8^+$ T cell population was elicited with specificity for an N-terminally extended epitope. Thus, the characteristic length, as well as the composition of MHC-I peptide cargo, is determined not only by the MHC-I peptide-binding groove but also by ERAAP proteolysis in the endoplasmic reticulum.

Proper control of a viral infection relies on recognition of virus-derived material by cytotoxic $CD8^+$ T cells. The $CD8^+$ T cells scan the cell surface for antigenic peptides presented by MHC class I molecules (pMHC-I) (1, 2). To facilitate immune surveillance, every nucleated cell generates thousands of peptides from self or foreign intracellular proteins. The MHC class I (MHC-I) molecules collect and chaperone the peptide cargo from the endoplasmic reticulum (ER) to the cell surface as potential ligands for the Ag receptors of $CD8^+$ T cells.

Address correspondence and reprint requests to Dr. Nilabh Shastri, Division of Immunology, LSA 421, Department of Molecular and Cell Biology, University of California, Berkeley, CA 94720-3200. nshastri@berkeley.edu.

Disclosures

The authors have no financial conflicts of interest.

The online version of this article has supplemental material in the text.

The peptide cargo for presentation by MHC-I is generated by the Ag-processing pathway (3). The pathway generally begins in the cytoplasm where precursor polypeptides are fragmented by the multicatalytic proteasome and other proteases (4,5). These proteolytic intermediates are then transported into the ER by cytosolic chaperones and the TAP. In the ER, the nascent MHC-I molecules acquire their peptide cargo in the peptide loading complex with the assistance of ER-resident chaperones, thiol reductases, and proteases (6-9). The peptide-loaded MHC-I then exit the ER and transit through the Golgi to the cell surface. Thus, the peptide pool available for presentation by MHC-I is subject to modification at various stages of the Ag-processing pathway.

The composition of the pMHC-I repertoire is believed to be determined primarily by peptide-binding properties of the MHC itself. High-resolution crystal structures of various pMHC-I complexes have shown that the peptide-binding groove of MHC-I is closed and with rare exceptions, accommodates only peptides with appropriate consensus motifs (10, 11). Moreover, the inability for cells to supply or load peptides in the ER because of inhibition or loss of cytoplasmic proteases (4, 12, 13), the TAP transporter (14) or components of the peptide-loading complex (15-17) results in loss of pMHC-I from the surface. In contrast, loss of the ER aminopeptidase associated with Ag processing (ERAP1 or ERAAP) had a relatively modest effect on expression of most pMHC-I on the cell surface (18). Yet, immunizations of ERAAP$^{-/-}$ mice with wild-type (WT) cells or vice versa, resulted in potent CD8^{+} T cell responses, suggesting that the pMHC-I repertoire was qualitatively changed (19). However, the extent and the nature of these differences have remained unclear.

In this study, we defined the molecular changes in the composition of the pMHC-I repertoire using complementary approaches. We analyzed amino acid sequences of a large number of peptides bound to H-2K^{b} and H-2D^{b} MHC-I molecules by tandem mass spectrometry (MS/MS). We also examined changes in individual peptides presented by MHC-I molecules in ERAAP$^{-/-}$ mice infected with mouse CMV (mCMV). With both approaches, we find that ER proteolysis defines the the composition and the structure of peptides presented by MHC-I molecules.

Materials and Methods

Mice and viruses

C57BL/6J (B6) and B10.D2-Hc^{1} H2^{d} H2-T18^{c}/nSnJ (B10.D2) mice were purchased from The Jackson laboratory (Bar Harbor, ME). B10.D2. ERAAP$^{-/-}$ (H-2^{d}) animals were obtained by crossing B6.ERAAP$^{-/-}$ (H-2^{b}) mice (18) with B10.D2 mice. For each MS experiment, 25 B6 and 25 B6.ERAAP$^{-/-}$ mice were used for spleen lysates preparation. For mCMV experiments, sex-matched B10.D2.ERAAP$^{+/-}$ heterozygous littermates and sex- and age-matched WT B10.D2 were used as controls. All mice were between 8 and 20 wk old and were maintained in accordance with the animal care and use regulations of the University of California and the University of Utah. Viral stocks of Smith strain mCMV were prepared as described in (20).

MS and peptide sequences

Peptide sequencing using immunoaffinity purification of pMHC complexes from detergent-solubilized spleen lysates was performed as described in (21). Briefly, freshly isolated splenocytes obtained from WT C57BL/6 and B6.ERAAP$^{-/-}$ mice were lysed and mixed with Sepharose beads covalently linked with mAbs Y-3 (anti–H-2K^{b}) (22) and B22.249 (anti–H-2D^{b}) (a gift from Dr. T.H. Hansen, Washington University, St. Louis, MO). H2-associated peptides eluted from each column were fractionated by HPLC and analyzed by

MS/MS (Agilent 6510 Q-TOF with Chip Cube ESI). Raw peptide data files generated were converted in Excel format (Microsoft, Redmond, WA), and sorted according to their corresponding m/z values, charge state, retention time, and intensity. A user-defined intensity threshold (7.0) above the background noise was fixed to limit false-positive identification. All identified peptides sequences above this score were manually verified and searched against the Swiss-Prot mouse protein database. In addition, peptides found in the fractions from C57BL/6 $\beta 2m^{-/-}$ mice (MHC-I–null) were considered contaminants and subtracted from the final list of peptides.

In vivo infection and immunization

Infections were performed by i.p. injection of 10^6 PFU of mCMV in PBS, unless otherwise indicated. Bone marrow-derived dendritic cell (BMDC) immunizations were performed as described in (23). Briefly, B10.D2. $ERAAP^{+/-}$ male BMDCs were activated for 24 h with 100 ng/ml LPS (Sigma-Aldrich, St. Louis, MO) and incubated with 1 mM synthetic peptide for 1.5 h. The 5×10^6 peptide-pulsed BMDCs were injected in the hind footpads of B10.D2.$ERAAP^{-/-}$ and WT B10.D2 mice in 50 μl PBS and $CD8^+$ T cell responses were assessed in the popliteal (draining) lymph node 7 d later.

Ex vivo cell preparations after viral infection

Mice were sacrificed 7–50 d postinfection. Spleens and lymph nodes were dissociated into single-cell suspensions in complete RPMI-1640 (Invitrogen, San Diego, CA) supplemented with 10% FCS (Thermo Scientific Hyclone, Logan, UT). Erythrocytes were depleted from the spleen using ACK lysis buffer (100 μM EDTA, 160 mM NH_4Cl, 10 mM $NaHCO_3$).

Generation of mCMV-specific T cell hybridomas

Spleens were harvested from WT and $ERAAP^{-/-}$ mice 7 d postinfection. WT and ERAAP-deficient splenocytes were restimulated weekly with 1 μM AI9 or DI10, respectively, using 3.5 krad-irradiated J774 BALB/c-derived macrophages as APCs. Recombinant human IL-2 (50 U/ml, BD Pharmingen, San Diego, CA) and 5% of T-stim (Thermo Fisher Scientific, Waltham, MA) were added after day 2 to support $CD8^+$ T cell proliferation. The proportion of peptide-specific $CD8^+$ T cells was monitored by intracellular IFN-γ staining after each restimulation. After three rounds of restimulation, responding cells were fused to the TCR-αβ–negative *lacZ*-inducible BWZ.36/CD8α fusion partner as described in (24). Specificity of the resulting hybridomas was tested by overnight incubation with peptide-pulsed or unpulsed J774. The TCR-mediated induction of β-galactosidase was quantified using the chromogenic substrate: chlorophenol red-β-D-galactopyranoside (CPRG, Roche, Basel, Switzerland). Cleavage of the CPRG by β-galactosidase releases a purple product, which absorbance was read at 595 nm, with a reference at 655 nm.

Plasmid constructs

The AI9 and DI10 peptides were introduced in the cytosol of transfected fibroblasts using an ubiquitin-based Ag release system as described (25). For each peptide sequence, the coding and noncoding DNA strands containing the appropriate SacII and BamHI cohesive ends, were annealed together and cloned in the pEGFP-Ub vector (gift from Dr. F. Lévy, University of Epalinges, Epalinges, Switzerland). $ERAAP^{-/-}$ tail fibroblasts were cotransfected with an $H\text{-}2D^d$-containing plasmid.

BMDCs and BM macrophages in vitro differentiation and infection

BMDCs were obtained from mouse femurs and tibias. DCs were differentiated with 10 ng/ml GM-CSF (BioSource International, Camarillo, CA) in complete RPMI-1640 for 6 d (purity: ~70% $CD11c^+$). BM macrophages (BMMs) were differentiated in Petri dishes with

RPMI-1640 supplemented with 20% FCS and 10% CSF-containing culture supernatant for 7 d (purity: ~95% $CD11b^+$). CSF-producing 3T3 cells were a gift from R. Vance, University of California, Berkeley, CA. BMMs were infected with mCMV at a multiplicity of infection of 0.5 for 24 h.

HPLC fractionation of peptide extracts from virus-infected cells

Peptides were extracted from 10^7 mCMV-infected or uninfected BMMs by boiling in 10% acetic acid solution. After centrifugation for 15 min at 16,000 × *g*, supernatants were filtered through 10 kDa Microcon filters. Filtrates were fractionated by HPLC on a C18 reverse-phase column (Vydac). Separation was achieved by a linear gradient of acetonitrile into water (10–30%) using 0.1% trifluoroacetic acid as the ion-pairing agent. Retention times of synthetic peptides spiked on uninfected cell extracts (prepared by D. King, University of California, Berkeley, CA) were determined using the same HPLC conditions.

Tetramer and Ab staining

All Abs were purchased from BD Biosciences (San Jose, CA). Surface labeling was performed according to standard procedures using FACS buffer (PBS, 3% FCS, 1 mM EDTA). PE-conjugated pMHC-I tetrameric complexes (tetramers) were a gift from S. Sierro and P. Klenerman, Oxford, UK. Allophycocyanin-conjugated tetramers were synthesized by the National Institutes of Health tetramer core facility. Peptides used were AGPPRYSRI (AI9), a H-$2D^d$–restricted peptide from the m164 ORF of mCMV, YPHFMPTNL (YL9), an H-$2L^d$–restricted peptide from the IE1 ORF of mCMV, and RPQASGVYM (NP118), an H-$2L^d$–restricted control peptide from the lymphocytic choriomeningitis virus nucleoprotein. Tetramer concentrations were optimized to maximize the signal/noise ratio. Typically, 10^6 cells were stained on ice sequentially with the tetramer, followed by CD8α. For FACS-based sorting, up to 5×10^7 cells were stained at a concentration of 4×10^7 cells/ml with the allophycocyanin-conjugated AI9-H-$2D^d$ tetramer. $CD8^+$ $tetramer^-$ cells were sorted with a Moflo cell sorter (Coulter Pharmaceutical, Seattle, WA) and checked for purity (<0.02% $allophycocyanin^+$ cells remained). Cells were further stained with the allophycocyanin-conjugated DI10-H-$2D^d$ tetramer. Flow cytometry data were acquired on a FC500 (Coulter) or LSRII (Becton Dickinson, San Jose, CA) cytometer and analyzed using the FlowJo software (TreeStar, Ashland, OR).

IFN-γ detection

IFN-γ production was triggered by in vitro stimulation with either 0.1 μM of exogenously added peptide, or peptide-pulsed APCs, or transfected $ERAAP^{-/-}$ fibroblasts, as indicated. When added together, AI9 and DI10 were used at 0.05 μM to achieve a 0.1 μM total peptide concentration. Control peptides, synthesized in the same conditions as the mCMV peptides, were TPHPARIGL (TL9), an H-$2L^d$–restricted epitope from β-galactosidase, and HPGSVNEFDF (HF10), an H-$2L^d$–restricted epitope from *Toxoplasma gondii*. IFN-γ was detected intracellularly using the Cytofix/Cytoperm kit (BD Biosciences) or on secretion using the mouse IFN-γ secretion assay (Miltenyi Biotec, Auburn, CA), according to the manufacturer's instructions. Briefly, cells were stimulated with exogenous AI9 in 12-W plates at 2×10^7 cells/well for 3 h. The 8×10^7 cells were labeled in 640 μl cold MACS buffer (PBS, 0.5% BSA, 2 mM EDTA) with 160 μl IFN-γ catch reagent before being allowed to secrete IFN-γ for 1 h at 37°C at 10^6 cells/ml. Cells were then labeled with 160 μl IFN-γ detection Ab, followed by 160 μl anti-PE microbeads. After 1 passage over a MACS LS column, purity of the negative fraction was assessed by FACS and IFN-γ–negative cells were further stimulated with the AI9 or DI10 peptide.

Degranulation assay

Spleen cells from mCMV-infected H-2^d mice were stimulated with 0.1 μM AI9 or DI10 in the presence of APC-coupled CD107a and CD107b Abs (1/20 dilution) as well as the monensin-containing GolgiStop reagent (BD Biosciences), which prevents internalization/recycling of surface CD107 molecules. After 5 h, cells were stained with CD8α and analyzed by flow cytometry to assess the proportion of CD8$^+$ cells that have degranulated during the assay.

Statistical analysis

Analyses were performed using the Prism software (GraphPad, San Diego, CA). The *p* values were calculated using the two-tailed unpaired *t* test (*$p < 0.05$; **$p < 0.005$).

Results

Longer peptides are bound to MHC-I in absence of ERAAP

To examine the impact of ER proteolysis in shaping the pMHC-I repertoire, we identified naturally processed peptides by mass-spectrometry in ERAAP$^{-/-}$ versus WT C57BL/6 mouse spleen cells. After affinity-purification, peptides were eluted from H-2K^b or H-2D^b and analyzed by MS/MS. A total of 298 and 299 distinct peptides bound to H-2D^b or H-2K^b MHC-I molecules respectively, were identified in 2 pooled independent experiments (Supplemental Tables 1 and 2).

To assess the qualitative differences in the pMHC-I repertoire in the presence or absence of ERAAP, we focused on the unique peptides presented by each MHC-I molecule in WT or ERAAP$^{-/-}$ cells. The sequenced peptides were plotted as vertical bars and grouped according to length (Fig. 1*A*). Among the 131 H-2D^b– and 138 H-2K^b–bound peptides in WT mice, 84% and 76% were, respectively, 9 and 8 aa long peptides in complete agreement with the original discovery of Rammensee and colleagues (26). The canonical lengths were, however, significantly altered in the absence of ERAAP (Fig. 1*A*, 1*B*). For both H-2D^b and H-2K^b MHC-I in ERAAP$^{-/-}$ cells, there was a decrease in recovery of peptides with the canonical length and a concomitant increase in longer peptides. Peptides longer than 10 and 9 residues for H-2D^b and H-2K^b increased from 16% to 57% and from 24% to 42%, respectively. In contrast, these differences in length distribution were not observed among the peptides shared by the two strains (Supplemental Fig. 1), further confirming the uniqueness of the peptide repertoire presented by MHC-I in ERAAP$^{-/-}$ cells.

To further characterize the changes in the pMHC-I repertoires, we analyzed the peptide sequences for the distribution of the conserved amino acids in WT-versus ERAAP-deficient cells. The logo representation shows the degree of conservation and the frequency of specific amino acid residues at each position of unique H-2D^b–bound (Fig. 2*A*, 2*B*) or H-2K^b–bound peptides (Supplemental Fig. 2*A*, 2*B*). As we and others have previously described (21, 26), the most conserved and frequent residues in H-2D^b–bound canonical 9 mers was an asparagine (N) at p5 position and an aliphatic residue (L, I, or M) at the C terminus (Fig. 2*A*). For H-2K^b–bound canonical 8 mers, the conserved residues were the aromatic phenylalanine (F) or tyrosine (Y) at p5 and an aliphatic residue (L, M, I, or V) at the C terminus (Supplemental Fig. 2*A*). Notably, the same consensus motifs were conserved in peptides of canonical length recovered from H-2D^b (9 mers) and H-2K^b (8 mers) MHC-I in ERAAP$^{-/-}$ cells (Fig. 2*B*, Supplemental Fig. 2*B*).

Remarkably, the same amino acids were also strongly conserved in at least half of the longer peptides isolated from MHC-I in WT and ERAAP$^{-/-}$ cells (Fig. 2*B*). Interestingly, the C-terminal anchor residue was highly conserved, whereas the extra residues were located at

either the C- or N-terminal side of the internal conserved anchor residues. For example, most of the 10 mer peptides isolated from the H-2D^b molecule contained the conserved aliphatic residue (e.g., L) at the C terminus and the N residue in the middle (Supplemental Table 1). Amino acid insertions at either side of the internal N or F/Y could thus cause "N- or C-bulges" in the conformation of H-2D^b– (Fig. 2*C*) or H-2K^b–bound peptides (Supplemental Fig. 2*C*).

In conclusion, the mass-spectrometry analysis clearly showed that the normal composition and canonical lengths of peptides presented by both H-2D^b and H-2K^b MHC-I was profoundly dependent on ERAAP.

CD8$^+$ T cell responses are altered in mCMV-infected ERAAP-deficient mice

Large scale analysis of MHC-I–bound peptides provides an overview of the peptide repertoire, but does not yield insights into the biological relevance of the observations. Thus, it was unclear whether the longer peptides in the immunoprecipitated material were actually present on the cell surface and whether the peptides elicited CD8$^+$ T cell responses. To determine how ERAAP influenced the presentation and immunogenicity, we used the mouse CMV as a model pathogen because the epitope specificity of CD8$^+$ T cells elicited by mCMV infection has been extensively characterized (27, 28). In WT mice of the H-2^d MHC haplotype, the primary and memory CD8$^+$ T cells recognize the YPHFMPTNL (YL9) peptide presented by H-2L^d and the AGPPRYSRI (AI9) peptide presented by H-2D^d MHC-I molecules. We infected H-2^d ERAAP-deficient (B10.D2.ERAAP$^{-/-}$), ERAAP-heterozygous (B10.D2.ERAAP$^{+/-}$), and WT (B10.D2) mice with mCMV. After 7 d, we determined the frequencies of YL9-H-2L^d and AI9-H-2D^d–specific CD8$^+$ T cells using pMHC-I tetramers (Fig. 3*A*, 3*B*). Relative to ERAAP$^{+/-}$ and ERAAP$^{+/+}$ mice, the proportion of CD8$^+$ T cells specific for the H-2L^d–restricted YL9 peptide reproducibly and significantly declined by ~25% in ERAAP$^{-/-}$ mice (4% versus 2.9%). In contrast, regardless of ERAAP expression, the frequency of CD8$^+$ T cells specific the AI9-H-2D^d complex did not change (Fig. 3*A*, 3*B*). We also measured the frequency of functional mCMV-specific CD8$^+$ T cells producing IFN-γ in response to YL9 or AI9 peptides (Fig. 3*C*). Again, the percentage of YL9-but not AI9-specific CD8 cells was lower in ERAAP$^{-/-}$ relative to ERAAP$^{+/-}$ or ERAAP$^{+/+}$ genotypes (Fig. 3*C*, 3*D*). Similar results were obtained postinfection with a 5-fold lower virus dose (Supplemental Fig. 3). Altogether, these results indicate that ERAAP deficiency alters the hierarchies of CD8$^+$ T cell responses toward antigenic peptides of mCMV.

mCMV-specific CD8$^+$ T cells recognize novel epitopes in ERAAP$^{-/-}$ mice

As seen previously, ERAAP-deficiency caused global changes in the pMHC-I repertoire. It was therefore possible that the altered specificity of mCMV-specific CD8$^+$ T cells could be due to structural changes in the naturally processed epitopes similar to those found in the pMHC-I repertoire in B6.ERAAP$^{-/-}$ cells (Figs. 1, 2). We tested the ability of mCMV-specific CD8$^+$ T cells to produce IFN-γ after stimulation with N-terminally extended versions of epitopes defined in WT mice (Fig. 4*A*, 4*B*). During acute (day 7) as well as latent phase of mCMV infection (day 50), similar percentage of CD8$^+$ T cells from WT or ERAAP$^{-/-}$ mice responded to YL9 or its N-terminally extended versions (Fig. 4*C*, Supplemental Fig. 4*A*). In contrast, a lower fraction of CD8$^+$ T cells from WT mice responded to the N-terminally extended versions than to the canonical AI9 peptide. Remarkably, a similar, if not somewhat higher, fraction of CD8$^+$ T cells from ERAAP$^{-/-}$ mice responded to N-terminally extended versions of the AI9 peptide (Fig. 4*D*, Supplemental Fig. 4*B*). The frequency of CD8$^+$ Tcells responding to N-terminally extended DI10 decamer versus the canonical AI9 nonamer, was higher with either WT or ERAAP$^{-/-}$ APCs ruling out potential differences in peptide-receptive MHC-I molecules on the cell

surface (Supplemental Fig. 5). Furthermore, the same results were obtained when the antigenic peptides were synthesized as ubiquitin fusion proteins and MHC-I were loaded endogenously in either WT or ERAAP$^{-/-}$ cells (Fig. 4*E*). Taken together, our data show that antiviral CD8$^+$ T cell were quantitatively, as well as qualitatively, altered in ERAAP$^{-/-}$ mice.

T-cell probes for detecting AI9-H-2D^d and DI10-H-2D^d complexes

The marked difference in responsiveness of CD8$^+$ T cells from WT versus ERAAP$^{-/-}$ mice to mCMV-derived AI9 peptide analogs suggested the existence of T cells with distinct ligand specificities. We enriched for such T cell clones by restimulating splenocytes from mCMV-infected ERAAP$^{-/-}$ or ERAAP$^{+/-}$ mice with either DI10 or AI9 peptides, respectively. The T cells were then fused with the BWZ.36/CD8 fusion partner to generate inducible β-galactosidase (lacZ)-expressing hybridomas as described previously (29). All the T cell hybrids obtained produced lacZ in response to the AI9 or the DI10 peptide (Fig. 5*A*, 5*B*). Most remarkably, titration of synthetic peptides showed that hybridoma AI9Z.3 from ERAAP$^{+/-}$ mice responded to AI9 as well as to DI10 peptide, albeit with a 3-fold lower sensitivity (Fig. 5*C*). In contrast, hybridoma DI10Z.1 from the ERAAP$^{-/-}$ mice responded only to the DI10 peptide and did not cross-react with the AI9 peptide even at 1000-fold higher concentration (Fig. 5*D*). Again, this difference in sensitivity was not due to differences in loading exogenous peptides, because it was observed with fibroblasts transfected with the ubiquitin fusion constructs (Fig. 5*E*, 5*F*). These results confirm that a subset of mCMV-specific CD8$^+$ T cells is elicited in ERAAP$^{-/-}$ mice with distinct ligand recognition properties.

Visualizing DI10-H-2D^d–specific CD8$^+$ T cells

We designed independent approaches to directly visualize the unique DI10-H-2D^d–specific population and estimate its actual frequency within the responding CD8$^+$ T cells. The inability of the DI10 peptide-specific hybridoma to recognize the AI9 peptide (Fig. 5), suggested that DI10-H-2D^d–specific CD8$^+$ T cells may not cross-react with AI9 in vivo either. It follows that, in presence of APCs pulsed with both AI9 and DI10, the number of unique DI10 peptide-specific CD8$^+$ T cells can be established by subtracting the number of cells that respond to the AI9 peptide alone from the total. Using IFN-γ production and degranulation (data not shown) assays, we found that DI10-H-2D^d–specific CD8$^+$ T cells comprised 0.6 ± 0.2% (mean ± SD, n = 3 experiments) of total CD8$^+$ T cells (Fig. 6*A*).

Taking further advantage of the lack of cross-reactivity of the DI10-H-2D^d–specific TCRs toward the AI9-H-2D^d pMHC-I ligand, we directly visualized the DI10-specific subset ex vivo. In the first approach, we stained CD8$^+$ T cells with an AI9-H-2D^d tetramer and selectively sorted the CD8$^+$ tetramer$^-$ population by flow cytometry to eliminate the AI9-H-2D^d–specific CD8$^+$ T cells. The sorted population was checked to ensure the depletion of AI9-H-2D^d tetramer$^+$ cells (Supplemental Fig. 6*A*, 6*B*). Subsequent staining of these cells with the DI10-H-2D^d tetramer revealed a distinct population in ERAAP$^{-/-}$ mice, representing ~0.4% of total CD8$^+$ cells (Fig. 6*B*), whereas DI10-H-2D^d tetramer$^+$ cells represented only ~0.1% of CD8$^+$ T cells from ERAAP$^{+/-}$ spleens (Fig. 6*C*). In the second independent approach, we stimulated splenocytes from infected mice with the AI9 peptide and selected cells that did not produce IFN-γ in response to AI9 stimulation (Fig. 6*D*, 6*E*). After confirming the depletion (Supplemental Fig. 6*C*, 6*D*), the non-responding cells were stimulated with DI10, or as a control, the original AI9 peptide. As expected, the proportion of CD8$^+$ T cells able to respond to AI9 after the second stimulation was profoundly decreased by >10-fold, but a clear and distinct ~1% of CD8$^+$ cells from ERAAP$^{-/-}$ mice specifically responded to DI10-H-2D^d (Fig. 6*D*). In sharp contrast, the proportion of CD8$^+$ T cells from ERAAP$^{+/-}$ spleens producing IFN-γ in response to DI10 was similar to the

background response against AI9 (Fig. 6*E*). Similar findings were obtained by assessing degranulation in splenocytes depleted from AI9-responding cells (Supplemental Fig. 7). In summary, these independent assays directly confirm and quantify the unique DI10-H-2D^d–specific CD8$^+$ T cell population, which represents between 0.5% and 1% of total CD8$^+$ T cells and preferentially expands in mCMV-infected mice lacking ERAAP.

Naturally processed DI10 is more abundant in the absence of ERAAP

Finally, we addressed the potential mechanisms responsible for generating this novel T cell subset in ERAAP$^{-/-}$ but not WT mice. It was possible that DI10-specific naive T cell precursors were present only in ERAAP$^{-/-}$ mice, and/or naturally processed DI10 peptide was produced more efficiently in the absence of ERAAP.

First, we determined whether WT mice could generate a T cell response against the noncanonical DI10 peptide. We immunized mice s.c. with BMDCs pulsed with DI10, or as a control, AI9 peptide. Seven days postimmunization, similar numbers of CD8$^+$ T cells were found in draining lymph nodes of ERAAP$^{-/-}$ and ERAAP$^{+/+}$ mice specific for DI10-H-2D^d (Fig. 7*A*). As expected, no DI10-H-2D^d–specific CD8$^+$ T cells were detected when mice were immunized with AI9-pulsed BMDCs (Supplemental Fig. 8*A*). In accordance with these data, staining of sorted CD8$^+$ AI9-H-2D^d tetramer$^-$ cells with the DI10-H-2D^d tetramer (according to a procedure described in Fig. 6*B*, 6*C*), revealed similar numbers of DI10-H-2D^d–specific CD8$^+$ T cells, whether ERAAP was present or not (Supplemental Fig. 8*B*). Altogether, these results indicate that the naive T cell repertoire of WT mice does contain CD8$^+$ T cells capable of responding to the DI10-H-2D^d ligand. Therefore, differences in the DI10-specific response during mCMV infection cannot be explained by innate differences in the T cell repertoire.

We next extracted naturally processed peptides from mCMV-infected BMMs. The extracts were fractionated by reverse phase-HPLC and each fraction was tested for its ability to stimulate the DI10Z.1 hybridomas (Fig. 5) to determine the amount of DI10 peptide present in each fraction. A unique peak of activity, with a retention time matching that of synthetic DI10, was found only in extracts of ERAAP$^{-/-}$ macrophages, but not in extracts of ERAAP$^{+/-}$ or ERAAP$^{+/+}$ macrophages (Fig. 7*B*, 7*C*). Thus, the processing outcome of the same antigenic precursors presented by the same H-2D^d MHC molecule was determined by ERAAP.

Discussion

In this study, we show that loss of ERAAP results in large-scale changes in the composition and structure of the pMHC-I repertoire derived from normal and viral proteins. These findings provide insights into why WT mice elicit potent CD8+ T cell responses to ERAAP-deficient cells and perhaps why ERAAP polymorphisms are associated with autoimmunity.

Previously, CD8$^+$ T cell responses elicited by reciprocal immunizations with cells from WT and ERAAP-deficient mice suggested that the pMHC-I repertoire produced in presence or absence of ER proteolysis contained some differences, the extent and nature of which remained unknown (19). In this study, we characterized the differences in the pMHC-I repertoire in WT and ERAAP-deficient H-2^b mice by mass-spectrometry methods used previously to determine the sequences of numerous peptides bound to human and mouse MHC-I (21, 30). Our analysis of the material eluted from the same H-2K^b and H-2D^b molecules in ERAAP$^{-/-}$ cells showed that a significant fraction of peptides were 1–4 aa longer than the canonical 8 (H-2K^b) or 9 (H2-D^b) aa. Thus, the increase in peptide-length is a major change in the pMHC-I repertoire of ERAAP-deficient cells and as a corollary, the

canonical length of a large number of peptide presented by MHC-I is clearly determined by ERAAP.

Remarkably, despite the increase in length of peptides found in ERAAP$^{-/-}$ cells, the C-terminal residue was conserved as an aliphatic amino acid (L, M, I, V, or F) in >92% and 82% of H-2D^{b}– and H-2K^{b}–bound peptides, respectively. This result establishes that the C termini of MHC-I–bound peptides are not generated by ERAAP and is consistent with the idea that C termini of antigenic peptides are produced in the cytoplasm prior to TAP-transport (31, 32). In addition to the conserved C termini, about half of the longer H-2D^{b} and H-2K^{b} peptides also contained the conserved asparagine and phenylalanine/tyrosine residues, respectively, suggesting that many extra residues can be accommodated within the consensus motifs (Fig. 2*C*, Supplemental Fig. 2*C*). In the longer H-2D^{b} peptides, extra residues were inserted either between the conserved asparagine and the C terminus or between the N terminus and the asparagine. How these peptides are bound to MHC molecules is not yet known, but assuming that the conserved residues serve similar MHC anchor functions in canonical and longer peptides, the peptides would be bound to MHC with either C-bulge or N-bulge (Fig. 2*C*). It is interesting to note that the general distribution of N-bulges and C-bulges was not found to be dramatically different between long peptides from ERAAP-deficient and WT cells (Fig. 2*C*, Supplemental Fig. 2*C*). This observation might indicate that the bulging conformation of those (infrequent) peptides found in WT cells largely resembles that of peptides from ERAAP-deficient cells. Furthermore, such bulges have been observed among EBV peptides presented by human HLA-B35 molecules (33). Crystallography of pMHC-I containing longer peptides identified in this study should reveal the actual structures (34). Taken together, the mass-spectrometry analysis showed that ERAAP was essential for maintaining the canonical length as well as the composition of peptides bound to MHC-I. Given that even subtle changes in peptide structure are sufficient to elicit CD8^{+} T cell responses (35), our data can now explain why structural changes in large numbers of pMHC-I caused by ERAAP-deficiency results in potent CD8^{+} T cell responses.

MS excels in providing simultaneous analysis of a large number of MHC-bound peptides. However, the knowledge of peptide sequences does not reveal whether the peptides are expressed on the cell surface and whether they are immunologically relevant in triggering CD8^{+} T cell responses. We therefore used mCMV, with well-defined antigenic epitopes in H-2^{d} mice, as a model pathogen to test the hypothesis that the repertoire of viral peptides presented by WT cells is disrupted in the absence of ERAAP. Our results indeed revealed several differences in generation and use of mCMV epitopes in ERAAP-deficient mice. In the absence of ERAAP, DI10, an N-terminally extended analog of the WT AI9 peptide, was naturally processed, loaded onto H-2D^{d} and was able to elicit virus-specific CD8^{+} T cell responses. As DI10 possesses the appropriate consensus motif for H-2D^{d} (X[G][P]XXXXX[I,L,F]) but is extended at the N terminus, it is likely to have an N-bulge conformation. Thus, our experiments provide an independent and physiological confirmation that proteolysis by ERAAP controls the length of MHC-I ligands and profoundly influences the epitope-specificity of the CD8^{+} T cell response.

Interestingly, ERAAP activity also influenced the magnitude of CD8^{+} T cell responses during mCMV infection. We observed a consistent drop in the frequency of CD8^{+} T cells specific for YL9-H-2L^{d} in ERAAP$^{-/-}$ mice. This significant difference supports the notion that ERAAP fine-tunes epitope hierarchies, as has been observed in other models of virus infection (36-38). Unlike those studies that tested only the canonical final peptides, we show that antiviral CD8^{+} T cell responses actually recognize structurally distinct pMHC-I in ERAAP$^{-/-}$ mice. Our observation questions whether these unusual CD8^{+} T cell responses can play a protective role in immunity against pathogens. So far, loss of ERAAP is known to

negatively impact protective immunity against *T. gondii* (23), but ERAAP$^{-/-}$ mice were able to control lymphocytic choriomeningitis virus infection as well as their WT counterpart (38). It should be interesting to revisit the virus infection models to test the existence of more CD8$^+$ T cell responses elicited by the longer unconventional peptides in ERAAP-deficient mice and to examine the protective function of these CD8$^+$ T cells.

Finally, the discovery of longer peptides bound to MHC-I with potentially bulged conformations brings up interesting questions as to their origins. Could these long peptides represent proteolytic intermediates that are trimmed by ERAAP into their final form? If the longer peptides were proteolytic intermediates, they should contain the typical consensus motif for MHC-I binding and N-terminal extensions as was the case for DI10, which is an N-terminally extended analog of the AI9 peptide. Surprisingly, the MS analysis showed that the majority of longer peptides present in H-2^b ERAAP$^{-/-}$ cells were likely bound in a C-bulge rather than an N-bulge conformation (Fig. 2). It is therefore possible that the trimming action of ERAAP can make the antigenic peptides “fit” for presentation by MHC-I by not only trimming extra N-terminal residues but also by other mechanisms. For example, the peptides in ERAAP-deficient cells, perhaps due to lower affinity for binding MHC-I, are outcompeted by higher-affinity peptides generated by ERAAP trimming. Alternatively, the peptides may dissociate more rapidly from MHC-I molecules and become susceptible to destruction by ERAAP as was shown recently for the SVL9 peptide that binds weakly to H-2D^b (39).

In conclusion, we find that ERAAP is an essential regulator of the optimal peptide repertoire presented by MHC-I, a task hitherto attributed only to tapasin-ERp57 in the peptide-loading complex within the ER (reviewed in Refs. 40, 41). The recent discovery that some ERAAP alleles are associated with autoimmunity in genomewide scans could be another dramatic manifestation of changes in the pMHC-I repertoire caused by ERAAP and MHC variants (42, 43).

Supplementary Material

Refer to Web version on PubMed Central for supplementary material.

Acknowledgments

We thank S. Sierro and P. Klenerman as well as the National Institutes of Health tetramer core facility for tetramers, H. Nolla and A. Valeros for cell sorting, D. King for peptide synthesis, N. Joncker for assistance with foot-pad injections, T. Hansen, F. Lévy, and R. Vance for useful reagents. We are grateful to N. An at the Center for Host-Pathogen Studies core facilities for assistance with virus preparations.

This work was supported by grants from the National Institutes of Health to N.S., funds from the ARUP Institute for Clinical and Experimental Pathology to J.D., a training grant from the California HIV/AIDS Research Program to F.D., fellowships from the Irvington Institute Fellowship program of the Cancer Research Institute to N.A.N., from the Japanese Society of the Promotion of Science to T.K., and from the International Human Frontier Science Program to N.B.

Abbreviations used in this paper:

BMDC	bone marrow-derived dendritic cell
BMM	BM macrophage
CPRG	chlorophenol red-β-D-galactopyranoside
ER	endoplasmic reticulum
ERAAP	ER aminopeptidase associated with Ag processing

mCMV	mouse CMV
MHC-I	MHC class I
MS	mass spectrometry
MS/MS	tandem mass spectrometry
pMHC-I	peptide-MHC-I complexes
WT	wild type

References

1. Shastri N, Cardinaud S, Schwab SR, Serwold T, Kunisawa J. All the peptides that fit: the beginning, the middle, and the end of the MHC class I antigen-processing pathway. Immunol. Rev. 2005; 207:31–41. [PubMed: 16181325]
2. Yewdell JW, Haeryfar SM. Understanding presentation of viral antigens to CD8+ T cells in vivo: the key to rational vaccine design. Annu. Rev. Immunol. 2005; 23:651–682. [PubMed: 15771583]
3. Shastri N, Schwab S, Serwold T. Producing nature's gene-chips: the generation of peptides for display by MHC class I molecules. Annu. Rev. Immunol. 2002; 20:463–493. [PubMed: 11861610]
4. Rock KL, Gramm C, Rothstein L, Clark K, Stein R, Dick L, Hwang D, Goldberg AL. Inhibitors of the proteasome block the degradation of most cell proteins and the generation of peptides presented on MHC class. Cell. 1994; 78:761–771. [PubMed: 8087844]
5. Kloetzel PM. Generation of major histocompatibility complex class I antigens: functional interplay between proteasomes and TPPII. Nat. Immunol. 2004; 5:661–669. [PubMed: 15224091]
6. Serwold T, Gaw S, Shastri N. ER aminopeptidases generate a unique pool of peptides for MHC class I molecules. Nat. Immunol. 2001; 2:644–651. [PubMed: 11429550]
7. Rock KL, York IA, Goldberg AL. Post-proteasomal antigen processing for major histocompatibility complex class I presentation. Nat. Immunol. 2004; 5:670–677. [PubMed: 15224092]
8. Garbi N, Hämmerling G, Tanaka S. Interaction of ERp57 and tapasin in the generation of MHC class I-peptide complexes. Curr. Opin. Immunol. 2007; 19:99–105. [PubMed: 17150345]
9. Cresswell P, Ackerman AL, Giodini A, Peaper DR, Wearsch PA. Mechanisms of MHC class I-restricted antigen processing and cross-presentation. Immunol. Rev. 2005; 207:145–157. [PubMed: 16181333]
10. Madden DR. The three-dimensional structure of peptide-MHC complexes. Annu. Rev. Immunol. 1995; 13:587–622. [PubMed: 7612235]
11. Speir JA, Stevens J, Joly E, Butcher GW, Wilson IA. Two different, highly exposed, bulged structures for an unusually long peptide bound to rat MHC class I RT1-Aa. Immunity. 2001; 14:81–92. [PubMed: 11163232]
12. Van Kaer L, Ashton-Rickardt PG, Eichelberger M, Gaczynska M, Nagashima K, Rock KL, Goldberg AL, Doherty PC, Tonegawa S. Altered peptidase and viral-specific T cell response in LMP2 mutant mice. Immunity. 1994; 1:533–541. [PubMed: 7600282]
13. Fehling HJ, Swat W, Laplace C, Kühn R, Rajewsky K, Müller U, von Boehmer H. MHC class I expression in mice lacking the proteasome subunit LMP-7. Science. 1994; 265:1234–1237. [PubMed: 8066463]
14. Van Kaer L, Ashton-Rickardt PG, Ploegh HL, Tonegawa S. TAP1 mutant mice are deficient in antigen presentation, surface class I molecules, and CD4-8+ T cells. Cell. 1992; 71:1205–1214. [PubMed: 1473153]
15. Grandea AG 3rd, Golovina TN, Hamilton SE, Sriram V, Spies T, Brutkiewicz RR, Harty JT, Eisenlohr LC, Van Kaer L. Impaired assembly yet normal trafficking of MHC class I molecules in Tapasin mutant mice. Immunity. 2000; 13:213–222. [PubMed: 10981964]
16. Garbi N, Tan P, Diehl AD, Chambers BJ, Ljunggren H-G, Momburg F, Hämmerling GJ. Impaired immune responses and altered peptide repertoire in tapasin-deficient mice. Nat. Immunol. 2000; 1:234–238. [PubMed: 10973281]

17. Garbi N, Tanaka S, Momburg F, Hämmerling GJ. Impaired assembly of the major histocompatibility complex class I peptide-loading complex in mice deficient in the oxidoreductase ERp57. Nat. Immunol. 2006; 7:93–102. [PubMed: 16311600]

18. Hammer GE, Gonzalez F, Champsaur M, Cado D, Shastri N. The aminopeptidase ERAAP shapes the peptide repertoire displayed by major histocompatibility complex class I molecules. Nat. Immunol. 2006; 7:103–112. [PubMed: 16299505]

19. Hammer GE, Gonzalez F, James E, Nolla H, Shastri N. In the absence of aminopeptidase ERAAP, MHC class I molecules present many unstable and highly immunogenic peptides. Nat. Immunol. 2007; 8:101–108. [PubMed: 17128277]

20. Gold MC, Munks MW, Wagner M, McMahon CW, Kelly A, Kavanagh DG, Slifka MK, Koszinowski UH, Raulet DH, Hill AB. Murine cytomegalovirus interference with antigen presentation has little effect on the size or the effector memory phenotype of the CD8 T cell response. J. Immunol. 2004; 172:6944–6953. [PubMed: 15153514]

21. Delgado JC, Escobar H, Crockett DK, Reyes-Vargas E, Jensen PE. Identification of naturally processed ligands in the C57BL/6 mouse using large-scale mass spectrometric peptide sequencing and bioinformatics prediction. Immunogenetics. 2009; 61:241–246. [PubMed: 19224205]

22. Hämmerling GJ, Rüsch E, Tada N, Kimura S, Hämmerling U. Localization of allodeterminants on H-2Kb antigens determined with monoclonal antibodies and H-2 mutant mice. Proc. Natl. Acad. Sci. USA. 1982; 79:4737–4741. [PubMed: 6181513]

23. Blanchard N, Gonzalez F, Schaeffer M, Joncker NT, Cheng T, Shastri AJ, Robey EA, Shastri N. Immunodominant, protective response to the parasite *Toxoplasma gondii* requires antigen processing in the endoplasmic reticulum. Nat. Immunol. 2008; 9:937–944. [PubMed: 18587399]

24. Malarkannan, S.; Mendoza, L.; Shastri, N. Generation of antigen-specific, lacZ-inducible T cell hybrids. In: Solheim, JC., editor. Methods in Molecular Biology. Antigen processing and presentation protocols. Humana Press; Totowa, New Jersey: 2000. p. 265-272.

25. Lévy F, Johnsson N, Rümenapf T, Varshavsky A. Using ubiquitin to follow the metabolic fate of a protein. Proc. Natl. Acad. Sci. USA. 1996; 93:4907–4912. [PubMed: 8643502]

26. Falk K, Rötzschke O, Stevanović S, Jung G, Rammensee H-G. Allele-specific motifs revealed by sequencing of self-peptides eluted from MHC molecules. Nature. 1991; 351:290–296. [PubMed: 1709722]

27. Sierro S, Rothkopf R, Klenerman P. Evolution of diverse antiviral CD8+ T cell populations after murine cytomegalovirus infection. Eur. J. Immunol. 2005; 35:1113–1123. [PubMed: 15756645]

28. Holtappels R, Thomas D, Podlech J, Reddehase MJ. Two antigenic peptides from genes m123 and m164 of murine cytomegalovirus quantitatively dominate CD8 T-cell memory in the H-2d haplotype. J. Virol. 2002; 76:151–164. [PubMed: 11739681]

29. Sanderson S, Shastri N. LacZ inducible, antigen/MHC-specific T cell hybrids. Int. Immunol. 1994; 6:369–376. [PubMed: 8186188]

30. Escobar H, Crockett DK, Reyes-Vargas E, Baena A, Rockwood AL, Jensen PE, Delgado JC. Large scale mass spectrometric profiling of peptides eluted from HLA molecules reveals N-terminal-extended peptide motifs. J. Immunol. 2008; 181:4874–4882. [PubMed: 18802091]

31. Cascio P, Hilton C, Kisselev AF, Rock KL, Goldberg AL. 26S proteasomes and immunoproteasomes produce mainly N-extended versions of an antigenic peptide. EMBO J. 2001; 20:2357–2366. [PubMed: 11350924]

32. Kunisawa J, Shastri N. The group II chaperonin TRiC protects proteolytic intermediates from degradation in the MHC class I antigen processing pathway. Mol. Cell. 2003; 12:565–576. [PubMed: 14527404]

33. Burrows JM, Bell MJ, Brennan R, Miles JJ, Khanna R, Burrows SR. Preferential binding of unusually long peptides to MHC class I and its influence on the selection of target peptides for T cell recognition. Mol. Immunol. 2008; 45:1818–1824. [PubMed: 17981331]

34. Tynan FE, Burrows SR, Buckle AM, Clements CS, Borg NA, Miles JJ, Beddoe T, Whisstock JC, Wilce MC, Silins SL, et al. T cell receptor recognition of a ‘super-bulged’ major histocompatibility complex class I-bound peptide. Nat. Immunol. 2005; 6:1114–1122. [PubMed: 16186824]

35. Mendoza LM, Paz P, Zuberi AR, Christianson G, Roopenian DC, Shastri N. Minors held by majors: the H13 minor histocompatibility locus defined as a peptide/MHC class I complex. Immunity. 1997; 7:461–472. [PubMed: 9354467]

36. Yan J, Parekh VV, Mendez-Fernandez Y, Olivares-Villagómez D, Dragovic S, Hill T, Roopenian DC, Joyce S, Van Kaer L. In vivo role of ER-associated peptidase activity in tailoring peptides for presentation by MHC class Ia and class Ib molecules. J. Exp. Med. 2006; 203:647–659. [PubMed: 16505142]

37. York IA, Brehm MA, Zendzian S, Towne CF, Rock KL. Endoplasmic reticulum aminopeptidase 1 (ERAP1) trims MHC class I-presented peptides in vivo and plays an important role in immunodominance. Proc. Natl. Acad. Sci. USA. 2006; 103:9202–9207. [PubMed: 16754858]

38. Firat E, Saveanu L, Aichele P, Staeheli P, Huai J, Gaedicke S, Nil A, Besin G, Kanzler B, van Endert P, Niedermann G. The role of endoplasmic reticulum-associated aminopeptidase 1 in immunity to infection and in cross-presentation. J. Immunol. 2007; 178:2241–2248. [PubMed: 17277129]

39. Kanaseki T, Shastri N. Endoplasmic reticulum aminopeptidase associated with antigen processing regulates quality of processed peptides presented by MHC class I molecules. J. Immunol. 2008; 181:6275–6282. [PubMed: 18941218]

40. Elliott T, Williams A. The optimization of peptide cargo bound to MHC class I molecules by the peptide-loading complex. Immunol. Rev. 2005; 207:89–99. [PubMed: 16181329]

41. Wearsch PA, Cresswell P. The quality control of MHC class I peptide loading. Curr. Opin. Cell Biol. 2008; 20:624–631. [PubMed: 18926908]

42. Burton PR, Clayton DG, Cardon LR, Craddock N, Deloukas P, Duncanson A, Kwiatkowski DP, McCarthy MI, Ouwehand WH, Samani NJ, et al. Wellcome Trust Case Control Consortium; Australo-Anglo-American Spondylitis Consortium (TASC); Biologics in RA Genetics and Genomics Study Syndicate (BRAGGS) Steering Committee; Breast Cancer Susceptibility Collaboration (UK). Association scan of 14,500 nonsynonymous SNPs in four diseases identifies autoimmunity variants. Nat. Genet. 2007; 39:1329–1337. [PubMed: 17952073]

43. Brown MA. Genetics and the pathogenesis of ankylosing spondylitis. Curr. Opin. Rheumatol. 2009; 21:318–323. [PubMed: 19496308]

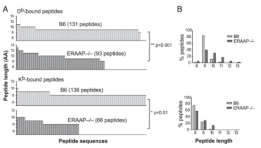

FIGURE 1.

Unusually long peptides are presented by MHC-I in the absence of ERAAP. *A*, Nonoverlapping B6 or ERAAP$^{-/-}$ specific peptides were represented as single vertical bars and plotted according to their amino acid length. Indicated *p* values between two groups were calculated by unpaired two-tailed *t* test based on the amino acid length. *B*, A different representation of the length distribution from all samples shown in *A*.

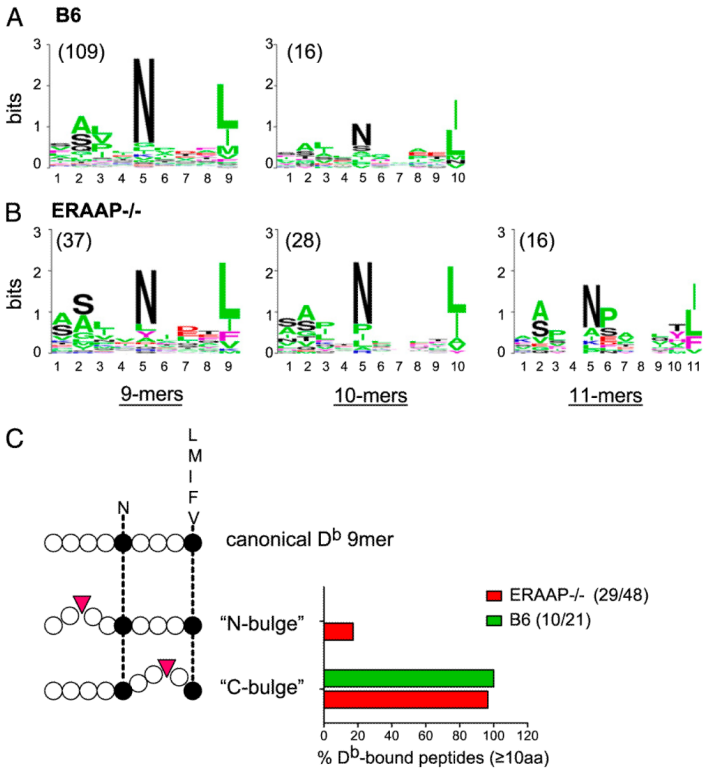

FIGURE 2.

ERAAP deficiency leads to presentation of longer bulging peptides. *A* and *B*, Logo representation of unique H-2D^b–bound (*A*) B6 or (*B*) ERAAP$^{-/-}$ peptide sequences analyzed independently according to their lengths shown on the *x*-axis. The height of each column is proportional to the degree of amino acid conservation and the height of each letter composing the column is proportional to its frequency at the given position. Numbers between parentheses indicate the number of peptide sequences analyzed. Groups containing less than 8 peptides (arbitrary choice) were not analyzed. Amino acids are colored as follows: acidic (red), basic (blue), hydrophobic (black), neutral (purple), and the others (green). *C*, Unusually long and unique peptides were tentatively sorted into two categories according to the location of the bulge: between the N terminus and the internal asparagine residue (N-bulge) or between the internal asparagine residue and the C terminus (C-bulge). See Supplemental Table 1 for peptide annotation. Bars show the fraction of peptides in each category. As some peptides could be classified in two categories, the sum of percentages may be higher than 100. Numbers between parentheses represent the number of peptides showing an apparent consensus motif (therefore included in the analysis) over the total number of longer and unique H-2D^b–bound peptides.

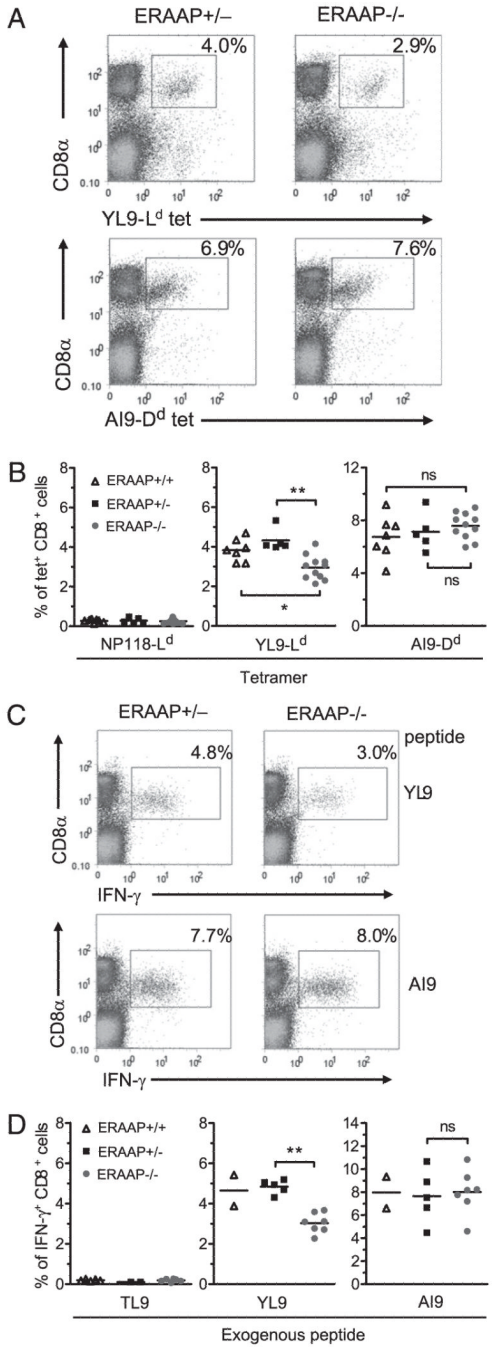

FIGURE 3.

Peptide specificity of $CD8^+$ T cell response to mCMV is altered in ERAAP-deficient mice. *A*, Seven days after i.p. infection, splenocytes from H-2^d ERAAP$^{+/-}$ and ERAAP$^{-/-}$ mice were costained with CD8 and the YL9-H-2L^d tetramer (*upper panels*) or the AI9-H-2D^d tetramer (*lower panels*). The percentage of tetramer$^+$ among all $CD8^+$ cells is indicated on the dot plots. *B*, Frequencies of $CD8^+$ cells stained with NP118-H-2L^d (a control tetramer), YL9-H-2L^d or AI9-H-2D^d tetramers. Each point represents an individual mouse. Data are pooled from two separate experiments. *C*, Seven days postinfection, IFN-γ production by splenocytes from H-2^d ERAAP$^{+/-}$ and ERAAP$^{-/-}$ mice was measured after restimulation with YL9 (*upper panels*) or AI9 (*lower panels*). Numbers on the dot plots represent the

percentage of IFN-γ^+ among all $CD8^+$ cells. *D*, Frequencies of $CD8^+$ cells producing IFN-γ in response to TL9 (an irrelevant H-$2L^d$ binding peptide), YL9 or AI9. Each point represents an individual mouse. Data are pooled from two separate experiments. *$p < 0.05$; **$p < 0.005$.

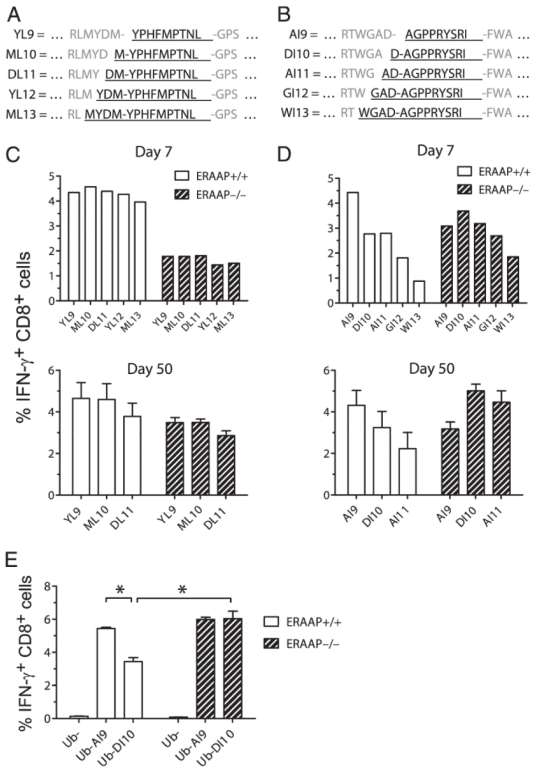

FIGURE 4.

$CD8^+$ T cell responses toward N-terminally extended peptides differ between $ERAAP^{-/-}$ and $ERAAP^{+/+}$ mice The amino acid sequences of peptide analogs of the (*A*) YL9 and (*B*) AI9 series, with the natural N-terminal extensions encoded by viral proteins IE1 and m164 are shown in bold and underlined. *C* and *D*, Synthetic peptides with these sequences were tested for their ability to stimulate IFN-γ production by splenocytes from WT or ERAAP-deficient mice infected 7 d (*top*) or 50 d (*bottom*) earlier with mCMV. Bars show the mean ± SEM of three spleens per genotype at day 50 and the value from five pooled spleens per genotype at day 7. Results represent three independent experiments. *E*, Seven days postinfection, IFN-γ production by splenocytes was measured in response to endogenously synthesized AI9 or DI10 peptides. APCs were $ERAAP^{-/-}$ fibroblasts cotransfected with $H\text{-}2D^d$ and a construct encoding ubiquitin fusion proteins for releasing AI9 or DI10 peptides in the cytoplasm (see *Materials and Methods*). Data represent two separate experiments with two to three mice per genotype. $*p < 0.05$.

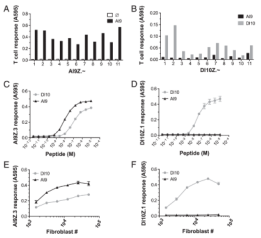

FIGURE 5.

Generation of T cell hybridomas specific for AI9-H-2D^{d} and DI10-H-2D^{d}. *A* and *B*, LacZ responses of CD8^{+} T cell hybridomas derived from mCMV-infected ERAAP$^{+/-}$ (*A*) and ERAAP$^{-/-}$ (*B*) mice. The hybridoma cells (AI9Z.~ or DI10Z.~) were cultured overnight with H-2^{d} J774 macrophages in absence or presence of synthetic AI9 or DI10 peptides. The lacZ activity was measured as the absorbance at 595 nm (A595) of a cleavage product of the CPRG substrate (29). *A*, A representative panel of 11 AI9-responding hybridomas (of 32 total) is shown. *B*, Only hybridomas with a higher reactivity to DI10 over AI9 are shown. *C* and *D*, The lacZ responses of (*C*) AI9Z.3 and (*D*) DI10Z.1 hybridomas to indicated concentrations of synthetic AI9 and DI10 peptides presented exogenously by J774 macrophages used as APCs. *E* and *F*, The lacZ responses of (*E*) AI9Z.3 and (*F*) DI10Z.1 hybridomas to ERAAP$^{-/-}$ fibroblasts expressing endogenously synthesized AI9 and DI10 precursors. Data (mean ± SEM) are from three different experiments and representative of the hybridomas shown in *A* and *B*.

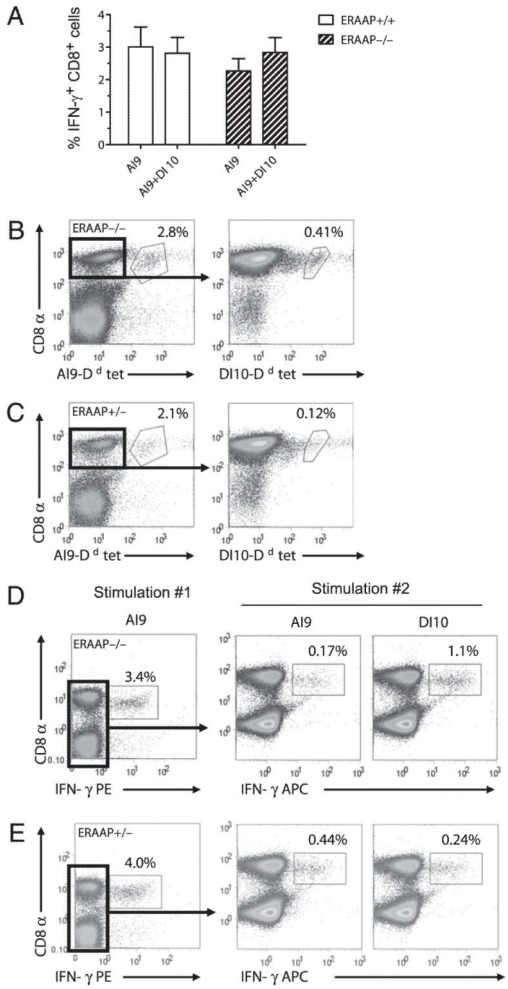

FIGURE 6.

The DI10-H-2D^{d}—specific CD8^{+} T cells are uniquely elicited in ERAAP$^{-/-}$ mice. *A*, Indirect quantification of DI10-H-2D^{d}–specific CD8^{+} T cells at day 7 postinfection. IFN-γ response by spleen cells from infected mice assessed after stimulation with exogenous AI9 or a mix of AI9 and DI10. The difference between both measurements corresponds to the frequency of genuine DI10-H-2D^{d}–specific CD8^{+} T cells. Data representative of three experiments. *B–E*, Direct visualization of DI10-H-2D^{d}–specific CD8^{+} T cells ex vivo. Seven days postinfection, splenocytes from (*B*) ERAAP$^{-/-}$ and (*C*) ERAAP$^{+/-}$ mice were costained with CD8 and the AI9-H-2D^{d} tetramer. CD8^{+} AI9-H-2D^{d} tetramer^{-} cells were FACS-sorted and further stained with DI10-H-2D^{d} tetramer (*right panels*). Numbers on dot plots show the percentage of tetramer^{+} of CD8^{+} cells. Results representative of two separate experiments with three spleens pooled per genotype. Splenocytes from mCMV-infected (*D*) ERAAP$^{-/-}$ and (*E*) ERAAP$^{+/-}$ mice were stimulated with synthetic AI9 and IFN-γ–producing cells were labeled, without fixation, using the Miltenyi IFN-γ secretion assay (*left panels*) (see *Materials and Methods*). IFN-γ–negative cells were sorted using magnetic beads. Following further stimulation with synthetic AI9 or DI10, IFN-γ production was monitored using a regular intracellular staining. Numbers show the percentage of IFN-γ^{+} of CD8^{+} cells. Data represent two experiments with three spleens pooled per genotype.

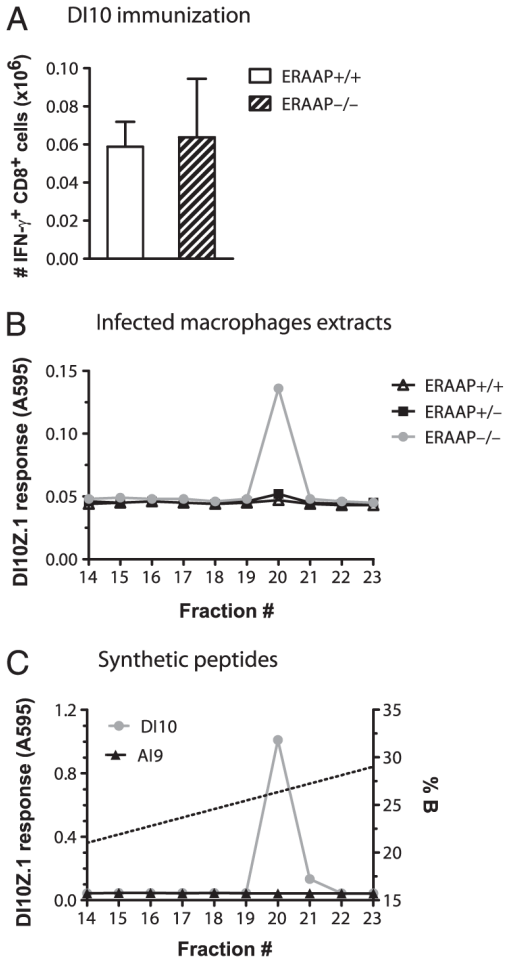

FIGURE 7.

Similar numbers of DI10-specific $CD8^+$ T cells induced by immunization but larger amounts of DI10 peptide produced in infected $ERAAP^{-/-}$ macrophages. *A*, Absolute numbers of DI10-H-$2D^d$–specific $CD8^+$ cells in lymph nodes 7 d after immunization with DI10-pulsed BMDCs. Numbers of IFN-γ–producing $CD8^+$ cells in response to AI9 alone or to a mix of AI9 and DI10 were measured. Bars show the difference between both responses. Mean ± SEM (n = 3 mice). Data representative of two independent experiments with 3–5 mice per group. *B*, Induction of β-galactosidase in DI10Z.1 hybridoma in response to mCMV-infected BMMs peptide extracts fractionated by reverse phase-HPLC. BMMs were infected for 24 h at multiplicity of infection 0.5. Each HPLC fraction was pulsed onto J774 macrophages that served as APCs. Buffer B (*right axis*) is acetonitrile containing 0.1% trifluoroacetic acid. *C*, LacZ response of DI10Z.1 hybridoma after fractionation of 1.5 pmoles of synthetic AI9 or DI10 using the same HPLC conditions as in *B*.